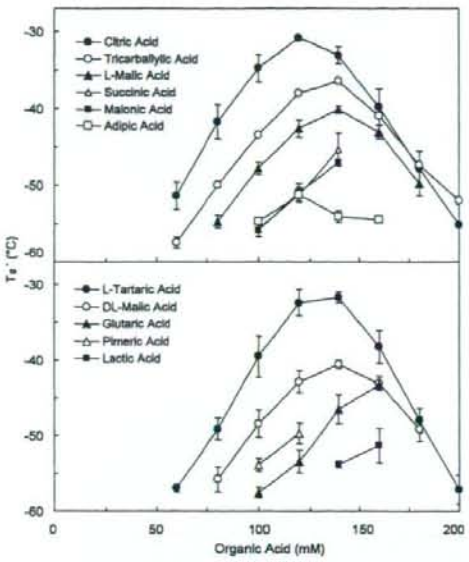

Fig. 4. Glass Transition Temperatures of the Maximally Freeze-Concentrated Phase (T_g') of Frozen Aqueous Solutions Containing 1,3-Diamino-2-hydroxypropane and Various Carboxylic Acids

Frozen solutions (10 μl, 200 mM total) were scanned from −70 °C at 5 °C/min (average±S.D., n=3).

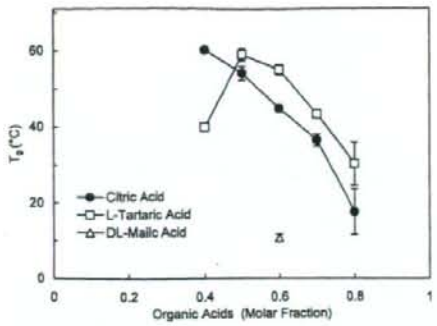

Fig. 5. Glass Transition Temperatures (T_g) of Freeze-Dried Solids Containing 1,3-Diamino-2-hydroxypropane and Organic Acids

The solids (1—2 mg) obtained by freeze-drying of aqueous solutions (200 mM total) were scanned from −30 °C at 5 °C/min (average±S.D., n=3).

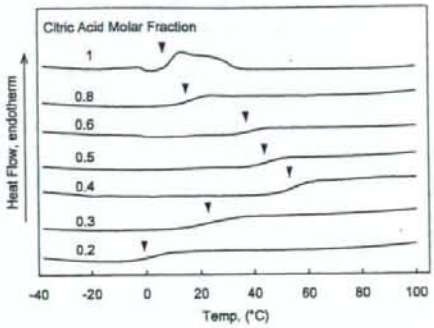

Fig. 6. Thermograms of Quench-Cooled Melt Mixture Solids Containing 1,3-Diamino-2-hydroxypropane and Citric Acid

The solids (1.5—2.5 mg) obtained by immersion of the heat-melt into liquid nitrogen were scanned from −30 °C at 5 °C/min.

acids (*e.g.*, succinic acid) and diamines (*e.g.*, diaminopropane) also suggested a large contribution of the hydroxyl groups to forming the high T_g' freeze-concentrated phase (data not shown).

Aqueous solutions containing 1,3-diamino-2-hydroxypropane and a hydroxy carboxylic acid (*e.g.*, DL-malic acid, L-tartaric acid, citric acid, 200 mM total) were freeze-dried to examine the physical properties of the resulting solids. The primary drying process at a shelf temperature (−40 °C) induced physical collapse in some lower T_g' (<−40 °C) samples, presumably because of the large molecular mobility of the freeze-concentrated phase.[9] Other frozen solutions were freeze-dried as cake-structure solids. Thermal analysis of the freeze-dried cake-structure mixture solids showed glass transitions (T_g) as high as 60.2 °C (Fig. 5, 120 mM 1,3-diamino-2-hydroxypropane, 80 mM citric acid). The solids freeze-dried from solutions containing 1,3-diamino-2-hydroxypropane and citric acid or L-tartaric acid at a 1 : 1 molar ratio showed amorphous components (halo patterns in the powder X-ray diffraction analysis) that have relatively high residual water (approx. 7—9%, w/w, data not shown). Amorphous solids of pure citric acid and 1,3-diamino-2-hydroxypropane were not available in the freeze-drying because of the physical collapse and crystallization that occurred during the process.

Quench-cooled heat-melt mixture solids containing 1,3-diamino-2-hydroxypropane and citric acid also showed a mixing-induced upward shift of the glass transition temperatures (Fig. 6). The highest transition temperature (54.5 °C) of the 0.4 citric acid molar fraction was slightly lower than that of the freeze-dried solid. Citric acid showed the glass transition of the quench-cooled solid at 9.5 °C.[10—12] The T_g of amorphous 1,3-diamino-2-hydroxypropane was not available using this method, and its low melting temperature (approx. 40—44 °C) strongly suggested a T_g below 0 °C (data not shown).

Mid-infrared analysis (FT-IR, KBr tablet transmission) of the amorphous mixture solids (0.5 citric acid molar fraction) prepared by freeze-drying and quench-cooling showed broad absorption bands (Fig. 7). Some relatively weak bands (*e.g.*, 1568 cm^{-1}) in the quench-cooled solid suggested evaporation of 1,3-diamino-2-hydroxypropane in the heating process. Non-destructive diffuse-reflection near-infrared (NIR) analysis of the freeze-dried mixture solids also showed broad bands typical for the amorphous solids (Fig. 8). Absence of some bands (*e.g.* N–H stretch 1st overtone of amino group at 6519 cm^{-1})[13] in the co-lyophilized solid (0.5 citric acid molar fraction) strongly suggested the interaction between the heterogeneous components that altered environment around the functional groups.

Discussion

Mixing of the alkyl diamines and hydroxy di- or tri-carboxylic acids induced high transition temperature amorphous concentrated phases in frozen aqueous solutions.[14] Some of the solute combinations formed cake-structure glass-state amorphous solids during freeze-drying. The high transition temperatures (T_g' and T_g) should allow faster drying processes at higher product temperature without physical collapse or shrinking of the solids.[9,15—17] Primary drying should

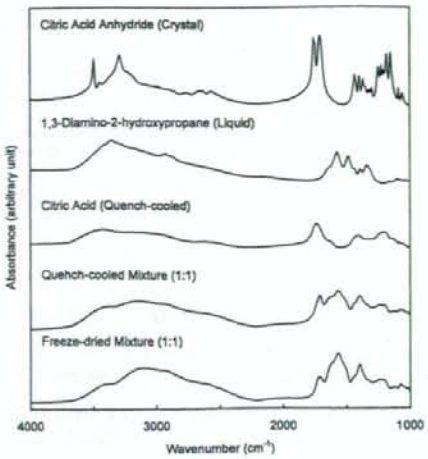

Fig. 7. FT-IR Spectra of Solids Containing 1,3-Diamino-2-hydroxypropane and Citric Acid

The mixture solids were obtained by quench-cooling of a melt (1 : 1 molar ratio, 165 °C, 3 min) or by freeze-drying of a solution (100 mM each).

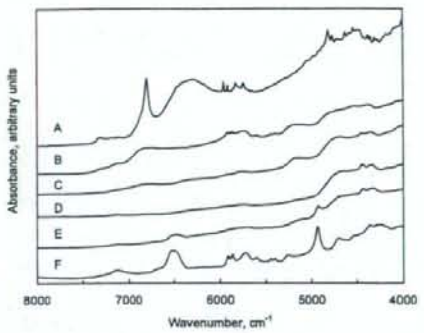

Fig. 8. Diffuse-Reflection Near-Infrared Spectra of Samples Containing 1,3-Diamino-2-hydroxypropane and Citric Acid

Each line denotes spectrum of anhydrous citric acid crystal powder (A), quench-cooled anhydrous citric acid melt (B), 1,3-diamino-2-hydroxypropane liquid (F), and solid lyophilized at the citric acid molar fraction of 0.3 (C), 0.5 (D), 0.7(E).

be conducted below the collapse temperature of the system (T_c), usually adjacent to and/or several degrees higher than the T_g', to obtain the pharmaceutically acceptable cake-structure solids. The primary drying is usually conducted at above −40 °C to accomplish ice sublimation on a practical timescale. Exposure of the partially dried solids above their glass transition temperature in the secondary drying process may shrink the cakes.

The bell-shaped profiles of the transition temperatures (T_g', T_g) depending on the component concentration ratio suggested strong attractive interaction between the components in the amorphous freeze-concentrated phase and the freeze-dried solids. Ideal mixing of nonionic molecules without particular attractive or repulsive interactions resulted in their glass transition at temperatures between those of the individual components, following the Gordon–Taylor equation.[11,18—20] It is also empirically known that frozen solutions containing the nonionic solute combinations have their thermal transition at temperatures (T_g') between those of individual solutes.[21,22] Significant upward deviation of the transition temperatures from those in the equation indicated the strong attractive interaction between the heterogeneous components. The mixing-induced transition temperature shift is also described as increasing "effective molecular weights" because many nonionic molecules (*e.g.*, polyols, saccharides) have the thermal transitions of the amorphous solids (T_g) or frozen solutions (T_g') at higher temperatures upon increasing the molecular weights.[23,24]

Networking of intense electrostatic interactions and hydrogen-bondings between the multiple functional groups should be a primary mechanism that raises the transition temperatures of the freeze-concentrated solute mixture phase and the freeze-dried solids.[4,6,25] The alkyl diamines and hydroxy di- or tri-carboxylic acids form ion pairs in aqueous solutions, and possibly in the freeze-concentrated phase. Some protonated polyamines selectively and strongly interact with particular dicarboxylates in aqueous solutions.[26] The ammonium carbohydrate ion pairs form multiple hydrogen-bonding in some non-polar solvents.[27,28] Continuous network of electrostatic interactions and hydrogen-bonding make the salt crystals popular supermolecular building blocks.[29] The differently protonated carboxyl and carboxylate groups also form an intermolecular hydrogen-bonding anion network.[30] It is plausible that the multi-component interactions contribute to the high transition temperature of the amorphous freeze-concentrated phase (T_g') and the freeze-dried solids (T_g). The eutectic crystallization observed in some high T_g' frozen solutions (*e.g.*, 60 mM diaminooctane and 140 mM L-tartaric acid) suggested effective interactions that induce the spatial ordering of the salt components above the transition temperature. Introduction of the hydroxyl groups to the components should provide additional hydrogen bonding in the amorphous phases. The limited effect of the component size on the transition temperatures also supported the significance of the interaction networks in determining physical properties.[23] Various factors, including the component structures, molar ratios, and water contents should alter the contribution of hydrogen-bonding and electrostatic (*e.g.*, ion–ion, ion–dipole, dipole–dipole) interactions in the amorphous phases. Further information on the interactions remains to be elucidated by other analytical methods (*e.g.*, solid-state NMR).

Recent studies on ionic liquids (RTMS: room temperature molten salt) also indicated the significant contribution of intermolecular (inter-ion) interactions to determining the physical properties of the locally disordered liquid or amorphous solid systems.[31,32] Factors that provide weak interaction between the molecules and/or ions (*e.g.*, size, charge distribution, functional groups) should induce low glass transition temperatures and low viscosities relevant to ionic liquids.[8] In contrast, glass-state solids would be designed by introducing strong interactions between the heterogeneous components.

The glass-state multi-component amorphous solids should be applicable in pharmaceutical formulations in several ways. Certain excipient mixture glass solids would become molecular dispersion matrixes that enable rapid dissolution of active ingredients or stabilization of biomacromolecules.[6] Some basic amino acids (*e.g.*, L-arginine) would be practical choices to form the glass-state mixture solids applicable in pharmaceutical formulations. The weakly acidic to alkaline pH of the high T_g mixtures and their re-hydrated solutions

would be preferable to ensure the storage stability of embedded molecules, as well as to reduce local stimulation in the site of parenteral application. Some pharmaceutically active ingredients (APIs) that have multiple amino or carboxyl groups may also form glass-state solids by direct interactions in mixing with some excipients.

References

1) Hancock B. C., Zografi G., *J. Pharm. Sci.*, **86**, 1—12 (1997).
2) Yu L., *Adv. Drug Deliv. Rev.*, **48**, 27—42 (2001).
3) Hilden L. R., Morris K. R., *J. Pharm. Sci.*, **93**, 3—12 (2004).
4) Tong P., Taylor L. S., Zografi G., *Pharm. Res.*, **19**, 649—654 (2002).
5) Tong P., Zografi G., *Pharm. Res.*, **16**, 1186—1192 (1999).
6) Izutsu K., Fujimaki Y., Kuwabara A., Aoyagi N., *Int. J. Pharm.*, **301**, 161—169 (2005).
7) Shalaev E. Y., Johnson-Elton T. D., Chang L., Pikal M. J., *Pharm. Res.*, **19**, 195—201 (2002).
8) Ohno H., *Bull. Chem. Soc. Jpn.*, **79**, 1665—1680 (2006).
9) Nail S. L., Jiang S., Chongprasert S., Knopp S. A., *Pharm. Biotechnol.*, **14**, 281—360 (2002).
10) Lu Q., Zografi G., *J. Pharm. Sci.*, **86**, 1374—1378 (1997).
11) Summers M. P., *J. Pharm. Sci.*, **67**, 1606—1610 (1978).
12) Timko R. J., Lordi N. G., *J. Pharm. Sci.*, **71**, 1185—1186 (1982).
13) Shenk J. S., Workman J. J., Jr., Westerhaus M. O., "Handbook of Near-Infrared Analysis," ed. by Burns D. A., Ciurczak E. W., Marcel Dekker, New York, 2001, pp. 419—474.
14) Akers M. J., Milton N., Byrn S. R., Nail S. L., *Pharm. Res.*, **12**, 1457—1461 (1995).
15) MacKenzie A. P., *Bull. Parenter. Drug Assoc.*, **20**, 101—130 (1966).
16) Tang X., Pikal M. J., *Pharm. Res.*, **21**, 191—200 (2004).
17) Akers M. J., Vasudevan V., Stickelmeyer M., *Pharm. Biotechnol.*, **14**, 47—127 (2002).
18) Gordon M., Taylor J. S., *J. Appl. Chem.*, **2**, 493—500 (1952).
19) Shamblin S. L., Taylor L. S., Zografi G., *J. Pharm. Sci.*, **87**, 694—701 (1998).
20) Hoppu P., Jouppila K., Rantanen J., Schantz S., Juppo A. M., *J. Pharm. Pharmacol.*, **2007**, 373—381 (2007).
21) Chang B. S., Randall C., *Cryobiology*, **29**, 632—656 (1992).
22) "Heat and Mass Transfer Issues in Freeze-Drying Process Development," ed. by Rambhatla S., Pikal M. J., American Association of Pharmaceutical Scientists, Arlington, 2004, pp. 75—109.
23) Levine H., Slade L., *J. Chem. Soc., Faraday Trans. 1*, **84**, 2619—2633 (1988).
24) Franks F., *Dev. Biol. Stand.*, **74**, 9—18 (1992).
25) Mattern M., Winter G., Kohnert U., Lee G., *Pharm. Dev. Technol.*, **4**, 199—208 (1999).
26) Hosseini M. W., Lehn J.-M., *Helv. Chim. Acta*, **69**, 587—603 (1986).
27) Yerger E. A., Barrow G. M., *J. Am. Chem. Soc.*, **77**, 6206—6207 (1955).
28) Sada K., Watanabe T., Miyamoto J., Fukuda T., Tohnai N., Miyata M., Kitayama T., Machara K., Ute K., *Chem. Lett.*, **33**, 160—161 (2004).
29) Sada K., Tani T., Shinkai S., *Synlett*, **2006**, 2364—2374 (2006).
30) Kobayashi N., Naito T., Inabe T., *Bull. Chem. Soc. Jpn.*, **76**, 1351—1362 (2003).
31) Fukumoto K., Yoshizawa M., Ohno H., *J. Am. Chem. Soc.*, **127**, 2398—2399 (2005).
32) Yamamuro O., Minamimoto Y., Inamura Y., Hayashi S., Hamaguchi H., *Chem. Phys. Lett.*, **423**, 371—375 (2006).

Feasibility of ^{19}F-NMR for Assessing the Molecular Mobility of Flufenamic Acid in Solid Dispersions

Yukio Aso,* Sumie Yoshioka, Tamaki Miyazaki, and Toru Kawanishi

National Institute of Health Sciences; 1–18–1 Kamiyoga, Setagaya, Tokyo 158–8501, Japan.
Received September 9, 2008; accepted October 22, 2008; published online October 23, 2008

The purpose of the present study was to clarify the feasibility of ^{19}F-NMR for assessing the molecular mobility of flufenamic acid (FLF) in solid dispersions. Amorphous solid dispersions of FLF containing poly(vinylpyrrolidone) (PVP) or hydroxypropylmethylcellulose (HPMC) were prepared by melting and rapid cooling. Spin–lattice relaxation times (T_1 and $T_{1\rho}$) of FLF fluorine atoms in the solid dispersions were determined at various temperatures (−20 to 150 °C). Correlation time (τ_c), which is a measure of rotational molecular mobility, was calculated from the observed T_1 or $T_{1\rho}$ value and that of the T_1 or $T_{1\rho}$ minimum, assuming that the relaxation mechanism of spin–lattice relaxation of FLF fluorine atoms does not change with temperature. The τ_c value for solid dispersions containing 20% PVP was 2—3 times longer than that for solid dispersions containing 20% HPMC at 50 °C, indicating that the molecular mobility of FLF in solid dispersions containing 20% PVP was lower than that in solid dispersions containing 20% HPMC. The amount of amorphous FLF remaining in the solid dispersions stored at 60 °C was successfully estimated by analyzing the solid echo signals of FLF fluorine atoms, and it was possible to follow the overall crystallization of amorphous FLF in the solid dispersions. The solid dispersion containing 20% PVP was more stable than that containing 20% HPMC. The difference in stability between solid dispersions containing PVP and HPMC is considered due to the difference in molecular mobility as determined by τ_c. The molecular mobility determined by ^{19}F-NMR seems to be a useful measure for assessing the stability of drugs containing fluorine atoms in amorphous solid dispersions.

Key words ^{19}F-NMR; molecular mobility; stability; crystallization; solid dispersion

Amorphous solid dispersions are used for improving the dissolution rate and solubility of poorly soluble drugs. However, drugs in amorphous form are generally less stable than crystalline drugs because of their higher energy state and higher molecular mobility. It is well known that polymeric excipients can reduce the crystallization rate of many amorphous drugs.[1—12] This stabilization by poly(vinylpyrrolidone) (PVP) is partly attributable to its ability to decrease molecular mobility, as indicated by increases in the glass transition temperature (T_g).[9] Therefore, it is of great interest to estimate the molecular mobility of drugs in solid dispersions. Although ^{13}C-NMR relaxation measurements are useful for assessing the molecular mobility of drugs in solid dispersions,[13] the low sensitivity of ^{13}C because of its low natural abundance is a drawback of ^{13}C-NMR. In contrast to ^{13}C, ^{19}F has very favorable sensitivity in NMR experiments, since it is present in 100% natural abundance, is second only to the proton in its resonance frequency (except ^{3}H) and has a spin quantum number of 1/2. The receptivity for ^{19}F is 83% of that for ^{1}H and 4700 times of that for ^{13}C.[14] Many drugs containing fluorine atoms are listed in The Japanese Pharmacopoeia. In contrast, almost all pharmaceutical excipients do not contain fluorine atoms. ^{19}F-NMR may therefore have an advantage over ^{13}C-NMR or ^{1}H-NMR for selectivity and sensitivity when assessing the molecular mobility of drugs containing fluorine atoms in pharmaceutical dosage forms such as solid dispersions.

The orientations and molecular mobility of flufenamic acid (FLF)[15] and ^{19}F-labeled α-tocopherol[16] in a lipid bilayer were studied using ^{19}F-NMR. Structures and molecular mobility of ^{19}F-labeled peptides and proteins in biological membranes were also investigated.[17—20] To the authors' knowledge, application of ^{19}F-NMR to studies of drug molecular mobility in solid dispersions has not been reported. This paper describes the feasibility of ^{19}F-NMR for assessing the molecular mobility of FLF in PVP or hydroxypropylmethylcellulose (HPMC) solid dispersions, and discusses the effect of polymer excipients on the crystallization tendency of FLF in solid dispersions in terms of differences in molecular mobility.

Experimental

Materials FLF (Fig. 1) was purchased from Wako Pure Chemical Industry (Osaka), and PVP and HPMC were from Sigma (St. Louis, MO, U.S.A.). FLF solid dispersions with PVP or HPMC were prepared by melting and cooling of mixtures of FLF with PVP or HPMC. The solid dispersions obtained were confirmed to be amorphous from microscopic observation under polarized light.

Nuclear Magnetic Relaxation Measurements ^{19}F-NMR measurements were carried out using a model JNM-MU25 pulsed NMR spectrometer (JEOL DATUM, Tokyo) operating at a resonance frequency of 25 MHz. Time profiles of spin–spin relaxation of the ^{19}F atoms of FLF were measured using the "solid echo" pulse sequence to overcome the dead time of the instrument. Spin–lattice relaxation time in the laboratory frame (T_1) was measured using the inversion recovery pulse sequence. Spin–lattice relaxation time in the rotating flame ($T_{1\rho}$) was measured at spin locking intensity of 10 G.

DSC Measurements T_g of FLF-PVP and FLF-HPMC solid dispersions was measured by DSC using a model 2920 differential scanning calorimeter and a refrigerator cooling system (TA Instruments, Newcastle, DE, U.S.A.). Approximately 5 mg of each solid dispersions was put into an aluminum sample pan and then sealed hermetically. T_g was measured at a heating rate of 20 °C/min. Temperature calibration of the instrument was carried out using indium.

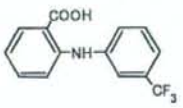

Fig. 1. Structure of FLF

* To whom correspondence should be addressed. e-mail: aso@nihs.go.jp

Results and Discussion

Molecular Mobility of FLF as Measured by ^{19}F-NMR Spin–Lattice Relaxation Time T_1 and $T_{1\rho}$ of fluorine atoms of FLF in PVP and HPMC solid dispersions were measured using a pulsed NMR spectrometer in the temperature range from −20 to 150 °C. T_1 is sensitive to the molecular motion on the time scale of the resonance frequency (MHz order). On the other hand, $T_{1\rho}$ is sensitive to the molecular motion with a frequency equivalent to the intensity of spin locking field (typically mid kHz order).[21] The temperature dependence of T_1 and $T_{1\rho}$ exhibits minimum at a specific temperature at which the molecules of interest have molecular motion with MHz time scale or mid kHz time scale predominantly. The resonance frequency of 25 MHz, lower than that of a conventional high resolution NMR spectrometer, was used to observe T_1 minimum in the temperature rage studied. Figure 2 shows the temperature dependence of T_1 and $T_{1\rho}$ of FLF fluorine atoms in PVP and HPMC solid dispersions. For FLF–PVP solid dispersions (7 : 3), the minimum of T_1 or $T_{1\rho}$ was observed at about 90 °C and 60 °C, respectively (Fig. 2A). When the PVP content decreased to 20% (w/w), T_1 and $T_{1\rho}$ of FLF at temperatures above 70 °C could not be determined due to rapid crystallization. Similar temperature dependence of T_1 or $T_{1\rho}$ was observed for the FLF–HPMC solid dispersions (Fig. 2B). The temperature difference between T_1 and $T_{1\rho}$ minimum is considered to be due to the difference in the time scale of molecular motion reflected on T_1 (MHz order) and $T_{1\rho}$ (mid kHz order). Since the molecular motion on MHz time scale becomes predominant at higher temperature than molecular motion on mid kHz time scale, T_1 minimum is observed at higher temperature than $T_{1\rho}$ minimum.

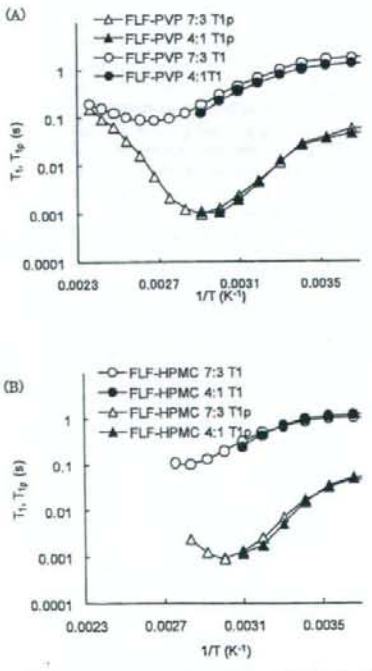

Fig. 2. Temperature Dependence of T_1 and $T_{1\rho}$ of FLF Fluorine Atoms in PVP (A) and HPMC (B) Solid Dispersions

We made following assumptions in order to estimate the molecular mobility of FLF from T_1 and $T_{1\rho}$ of FLF fluorine atoms: first, we assumed that FLF fluorine atoms in the solid dispersions relaxes mainly *via* dipolar interaction, and that the contribution of the spin–rotation interaction mechanism[21] is negligible. While relaxation *via* the spin–rotation interaction mechanism has been reported for liquid sample,[22–24] complete domination of dipolar interactions has been reported for fluorine atoms for polycrystalline van der Waals molecular solid.[25] We also made an assumption that the contribution of the cross-relaxation between fluorine and proton atoms can be considered small. It is known that relaxation is not intrinsically single-exponential when cross-relaxation between fluorine and proton atoms takes place.[14] However, we assumed small contribution of the cross-relaxation, because the relaxation of FLF fluorine atoms in the solid dispersions was exponential within experimental uncertainty. In studies of molecular motions, a large number of models describing molecular motions have been proposed for calculation of the spectrum density function.[26] We used a simple model that the molecular motion reflected on T_1 or $T_{1\rho}$ is represented by single correlation time for the purpose of comparing the mobility of FLF in the PVP and HPMC solid dispersions. According to the above assumptions, T_1 and $T_{1\rho}$ are described by Eqs. 1 and 2.[21]

$$\frac{1}{T_1} = \frac{6}{20}\frac{\gamma^4\hbar^2}{r^6}\left\{\frac{\tau_c}{1+\omega_0^2\tau_c^2} + \frac{4\tau_c}{1+4\omega_0^2\tau_c^2}\right\} \quad (1)$$

$$\frac{1}{T_{1\rho}} = \frac{3}{20}\frac{\gamma^4\hbar^2}{r^6}\left\{\frac{3\tau_c}{1+4\omega_1^2\tau_c^2} + \frac{5\tau_c}{1+\omega_0^2\tau_c^2} + \frac{2\tau_c}{1+4\omega_0^2\tau_c^2}\right\} \quad (2)$$

where τ_c is the correlation time that characterizes molecular reorientations, and ω_0 and ω_1 are the resonance frequencies of fluorine atoms in the static magnetic field and spin locking field, respectively. γ, r and $\hbar$ are the gyromagnetic ratio of fluorine, the distance of neighboring fluorine atoms, and the Plank constant divided by 2π, respectively. Equations 1 and 2 infer that T_1 and $T_{1\rho}$ become minimal when $\omega_0\tau_c$ is approximately 0.62[27] and $\omega_1\tau_c$ is approximately 0.52,[21] respectively. When the minimum of T_1 or $T_{1\rho}$ is observed, we can calculate the unknown value, r, in Eqs. 1 and 2. If r is known, the τ_c value can be calculated from the observed T_1 or $T_{1\rho}$ value, assuming that r does not change with temperature.

The values of r calculated from the T_1 and $T_{1\rho}$ minimum observed for the FLF–PVP solid dispersion (7 : 3) were 2.3 and 2.4 Å, respectively, and similar r values were obtained for the FLF–HPMC solid dispersion (7 : 3). These values are comparable to the reported value (2.174 Å) for 3-(trifluoromethyl)phenanthrene,[25] indicating that dipole interaction between neighboring fluorine atoms can be considered the predominant relaxation mechanism of FLF fluorine atoms in the solid dispersions. The difference between the r values obtained in this work and the reported value suggests that the possibility of the spin–rotation interaction mechanism and/or dipole interaction between fluorine and proton atoms cannot be excluded as a relaxation mechanism of FLF fluorine atoms.

Figure 3 shows the temperature dependence of τ_c calculated from T_1 and $T_{1\rho}$ for FLF fluorine atoms in the solid dis-

persions. The τ_c of FLF fluorine atoms in PVP solid dispersions calculated from $T_{1\rho}$ was 8.2 μs at 50 °C, which was about 3 times larger than that in HPMC solid dispersions (2.6 μs), indicating that the molecular mobility of FLF was lowered more strongly by PVP than by HPMC.

The τ_c values calculated using T_1 values differ from those calculated from $T_{1\rho}$ values. The slope of temperature dependence of τ_c changed around T_g. These findings suggest that the assumption that the molecular motion reflected on T_1 and $T_{1\rho}$ is represented by a single τ_c may be too simple to describe the molecular motion of FLF in the solid dispersions at temperatures studied, and that two or more molecular motions, such as rotation of trifluoromethyl group and motions with larger scales than rotation of trifluoromethyl group, may be reflected on T_1 and $T_{1\rho}$. Further studies including ^{1}H-NMR relaxation measurement and dielectric relaxation measurements will be needed to identify the detailed molecular motion of FLF in the solid dispersions.

Correlation between Crystallization Tendency and Molecular Mobility of FLF in Solid Dispersions Crystallization proceeds *via* formation of crystal nuclei and crystal growth. As a measure of the crystallization tendency of amorphous FLF in solid dispersions, the overall crystallization rate of amorphous FLF in the solid dispersions was estimated from the time profiles amorphous FLF remaining in the solid dispersions instead of measuring the nucleation rate and growth rate. Amorphous FLF remaining in the solid dispersions was estimated by analyzing solid echo signals of FLF fluorine atoms. Figure 4 shows the solid echo signal of fluorine atoms of FLF in solid dispersions containing 20% (w/w) PVP and that of fluorine atoms of crystalline FLF. The signal for the solid dispersions was describable by the Lorentzian relaxation equation (Eq. 3), and its relaxation time (T_{2L}) was approximately 140 μs. Crystalline FLF exhibited Gaussian relaxation signals (Eq. 4), and its relaxation time (T_{2G}) was approximately 30 μs. These results indicate that amorphous FLF in solid dispersions is considered to exhibit Lorentzian relaxation signals.

$$I=I_0\exp(-t/T_{2L}) \tag{3}$$

$$I=I_0\exp\{-t^2/(2T_{2G}^2)\} \tag{4}$$

where I_0 and I represent the signal intensities at time 0 and t, respectively. Figure 5 shows solid echo signals for the fluorine atoms of FLF in the solid dispersions stored at 60 °C. Samples stored at 60 °C exhibited biphasic decay signals, and signals were describable by summation of the Gaussian (solid line) and Lorentzian (dashed line) equations (Eq. 5).

$$I=I_0\{P_L\exp(-t/T_{2L})+P_G\exp(-t^2/2T_{2G}^2)\} \tag{5}$$

where P_L and P_G are the ratio of fluorine atoms exhibiting Lorentzian and Gaussian relaxation process, respectively, and $P_L+P_G=1$. Assuming that the T_{2L} and T_{2G} values are 140 and 30 μs, respectively, P_L values of FLF in the solid dispersions were estimated by curve fitting. P_L values of the solid dispersions decreased with increasing storage time, indicating that crystallization of amorphous FLF in solid dispersions takes place during storage at 60 °C. To certify the reliability of the P_L values obtained by ^{19}F-NMR measurements, change in the heat capacity at T_g ($\Delta C_p(T_g)$) was determined for the solid dispersions stored at 60 °C for various periods as a measure of amorphous FLF remaining, and was compared with the value of P_L. As shown in Fig. 6, the P_L value was proportional to the $\Delta C_p(T_g)$ value, and was considered to be a useful measure of amorphous FLF remaining in the solid dispersions.

Figure 7 shows the time profiles of the P_L values for FLF solid dispersions containing 20% (w/w) PVP or HPMC at 60 °C. The decrease in the ratio of Lorentzian fluorine atoms was faster for HPMC solid dispersions than for PVP solid dispersions, indicating that the overall crystallization rate of FLF in HPMC solid dispersions is larger than that in PVP solid dispersions. The overall crystallization rate depends on both molecular mobility (the rate of diffusion across the interface between crystalline and amorphous phase) and ther-

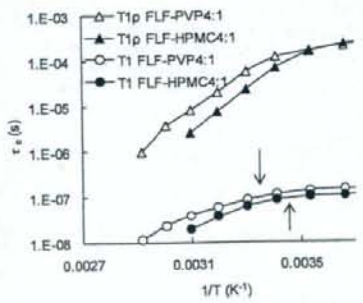

Fig. 3. Temperature Dependence of τ_c of FLF Fluorine Atoms in PVP and HPMC Solid Dispersions

Arrows in the figure represent T_g.

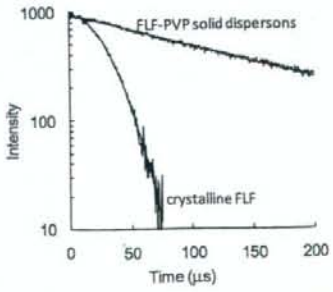

Fig. 4. Typical Solid Echo Signal of Fluorine Atoms of FLF in the Freshly Prepared Solid Dispersion Containing 20% (w/w) PVP and That of Fluorine Atoms of Crystalline FLF

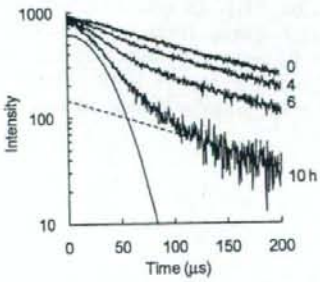

Fig. 5. Typical Solid Echo Signals of Fluorine Atoms of FLF in the Solid Dispersions Containing 20% (w/w) PVP Stored at 60 °C

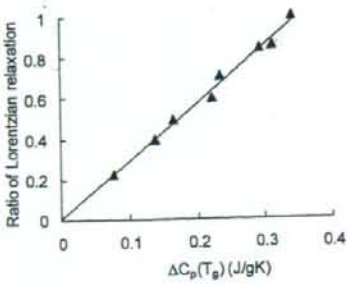

Fig. 6. The Ratio of FLF Fluorine Atoms Exhibiting Lorentzian Relaxation as a Function of Changes in the Heat Capacity at T_g

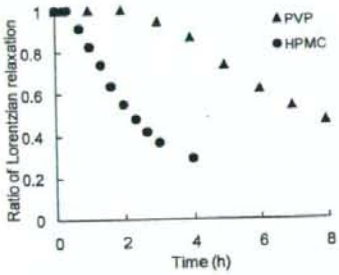

Fig. 7. Time Profiles of the Ratio of FLF Fluorine Atoms Exhibiting Lorentzian Relaxation in PVP and HPMC Solid Dispersions Stored at 60 °C

modynamic factors, such as free energy difference between crystalline and amorphous form.[2,3,10] Differences in the overall crystallization rate of amorphous FLF are consistent with those in the molecular mobility (Fig. 3), suggesting that the molecular mobility as determined by the ^{19}F-NMR spin–lattice relaxation times may be one of the factors determining crystallization rate, and useful as a measure of the physical stability of FLF in solid dispersions. The T_g values of the solid dispersions containing 20% PVP and 20% HPMC were 23 °C and 15 °C, respectively, indicating that molecular mobility reflected on T_g is higher for the solid dispersion containing HPMC than for that containing PVP. The T_g data seem to support the speculation obtained from NMR data. However, the scale of molecular mobility reflected on T_g is considered to be larger than that reflected on τ_c. Further studies should be conducted to elucidate the quantitative correlation between the physical stability of amorphous FLF and the molecular mobility determined by ^{19}F-NMR.

In conclusion, ^{19}F-NMR is useful for elucidating the molecular mobility of drugs containing fluorine atoms in amorphous solid dispersions. τ_c values of FLF fluorine atoms were calculated from the ^{19}F-NMR spin–lattice relaxation data. The τ_c value for solid dispersions containing 20% PVP was 2—3 times longer than that for solid dispersions containing 20% HPMC at 50 °C. Molecular mobility of FLF in the solid dispersions containing 20% PVP was lower than in those containing 20% HPMC, and this was consistent with the fact that the overall crystallization rate of amorphous FLF in the solid dispersion containing PVP was smaller than in that containing HPMC. The molecular mobility determined by ^{19}F-NMR seems to be useful as a measure of the physical stability of an amorphous drug in solid dispersions.

Acknowledgements Part of this work was supported by a Grant-in-aid for Research on Publicly Essential Drugs and Medical Devices from The Japan Health Sciences Foundation.

References

1) Yoshioka M., Hancock B. C., Zografi G., *J. Pharm. Sci.*, **84**, 983—986 (1995).
2) Matsumoto T., Zografi G., *Pharm. Res.*, **16**, 1722—1728 (1999).
3) Crowley K. J., Zografi G., *Pharm. Res.*, **20**, 1417—1422 (2003).
4) Shamblin S. L., Huang E. Y., Zografi G., *J. Therm. Anal.*, **47**, 1567—1579 (1996).
5) Shamblin S. L., Zografi G., *Pharm. Res.*, **16**, 1119—1124 (1999).
6) Zeng X. M., Martin G. P., Marriott C., *Int. J. Pharm.*, **218**, 63—73 (2001).
7) Miyazaki T., Yoshioka S., Aso Y., Kojima S., *J. Pharm. Sci.*, **93**, 2710—2717 (2004).
8) Khougaz K., Clas S., *J. Pharm. Sci.*, **89**, 1325—1334 (2000).
9) Berggren J., Alderborn G., *Eur. J. Pharm. Sci.*, **21**, 209—215 (2004).
10) Aso Y., Yoshioka S., Kojima S., *J. Pharm. Sci.*, **93**, 384—391 (2004).
11) Miyazaki T., Yoshioka S., Aso Y., *Chem. Pharm. Bull.*, **54**, 1207—1210 (2006).
12) Konno H., Taylor L. S., *J. Pharm. Sci.*, **95**, 2692—2705 (2006).
13) Aso Y., Yoshioka S., *J. Pharm. Sci.*, **95**, 318—325 (2006).
14) Harris R. K., Monti G. A., Holstein P., "Solid State NMR of Polymers," Chap. 6, ed. by Ando I., Asakura T., Elsevier, Amsterdam, 1998, pp. 351—414.
15) Grage S. L., Ulrich A. S., *J. Magn. Reson.*, **146**, 81—88 (2000).
16) Urano S., Matsuo M., Sakanaka T., Uemura I., Koyama M., Kumadaki I., Fukuzawa K., *Arch. Biochem. Biophys.*, **303**, 10—14 (1993).
17) Afonin S., Glaser R. W., Berditchevskaia M., Wadhwani P., Gührs K. H., Möllmann U., Perner A., Ulrich A. S., *ChemBioChem*, **4**, 1151—1163 (2003).
18) Salgado J., Grage S. L., Kondejewski L. H., Hodges R. S., McElhaney R. N., Ulrich A. S., *J. Biomol. NMR*, **21**, 191—208 (2001).
19) Williams S. P., Haggie P. M., Brindle K. M., *Biophys. J.*, **72**, 490—498 (1997).
20) Quint P., Ayala I., Busby S. A., Chalmers M. J., Griffin P. R., Rocca J., Nick H. S., Silverman D. N., *Biochemistry*, **45**, 8209—8215 (2006).
21) Farrar T. C., Breker E. D., "Pulse and Fourier Transform NMR," Academic Press, New York and Lodon, 1971.
22) Namgoong H., Lee J. W., *Bull. Korean Chem. Soc.*, **14**, 91—95 (1993).
23) Huang S.-G., Rogers M. T., *J. Chem. Phys.*, **68**, 5601—5606 (1978).
24) Gutowsky H. S., Lawrenceson I. J., Shimomura K., *Phys. Rev. Lett.*, **6**, 349—351 (1961).
25) Beckmann P. A., Rosenberg J., Nordstrom K., Mallory C. W., Mallory F. B., *J. Phys. Chem. A*, **110**, 3947—3953 (2006).
26) Horii F., "Solid State NMR of Polymers," Chap. 3, ed. by Ando I., Asakura T., Elsevier, Amsterdam, 1998, pp. 51—82.
27) Ruan R. R., Chen P. L., "Water in Foods and Biological Materials," Chap. 7, Technomic Publishing Co., Lancaster Basel, 1998, pp. 253—278.

Freeze-Drying of Proteins in Glass Solids Formed by Basic Amino Acids and Dicarboxylic Acids

Ken-ichi IZUTSU,*[,a] Saori KADOYA,[b] Chikako YOMOTA,[a] Toru KAWANISHI,[a] Etsuo YONEMOCHI,[b] and Katsuhide TERADA[b]

[a] *National Institute of Health Sciences; 1–18–1 Kamiyoga, Setagaya, Tokyo 158–8501, Japan: and* [b] *Faculty of Pharmaceutical Sciences, Toho University; 2–2–1 Miyama, Funabashi, Chiba 274–8510, Japan.*
Received August 1, 2008; accepted October 11, 2008; published online October 15, 2008

The purpose of this study was to produce and characterize glass-state amorphous solids containing amino acids and organic acids that protect co-lyophilized proteins. Thermal analysis of frozen solutions containing a basic amino acid (*e.g.*, L-arginine, L-lysine, L-histidine) and a hydroxy di- or tricarboxylic acid (*e.g.*, citric acid, L-tartaric acid, DL-malic acid) showed glass transition of maximally freeze-concentrated solute at temperatures (T_g') significantly higher than those of the individual solute solutions. Mixing of the amino acid with some dicarboxylic acids (*e.g.*, oxalic acid) also suggested an upward shift of the transition temperature. Contrarily, combinations of the amino acid with monocarboxylic acids (*e.g.*, acetic acid) had T_g's between those of the individual solute solutions. Co-lyophilization of the basic amino acids and citric acid or L-tartaric acid resulted in amorphous solids that have glass transition temperatures (T_g) higher than the individual components. Mid- and near-infrared analysis indicated altered environment around the functional groups of the consisting molecules. Some of the glass-state excipient combinations protected an enzyme (lactate dehydrogenase, LDH) from inactivation during freeze-drying. The glass-state excipient combinations formed by hydrogen-bonding and electrostatic interaction network would be potent alternative to stabilize therapeutic proteins in freeze-dried formulations.

Key words freeze-drying; protein formulation; amorphous; stabilization; glass

Freeze-drying is a popular method of ensuring the stability of proteins that are not stable enough in aqueous solutions during the period required for storage and distribution.[1,2] Various freeze-dried protein formulations contain excipients (*e.g.*, sugars, polymers, and amino acids) that protect proteins from physical and chemical changes. Disaccharides (*e.g.*, sucrose, trehalose) are the most popular among them because they stabilize proteins both thermodynamically and kinetically in aqueous solutions and freeze-dried solids.[3—5]

The development of freeze-dried protein formulations containing amino acids is often more challenging than the development of formulations with saccharides because of the varied physical and chemical properties (*e.g.*, crystallinity, glass transition temperature) of the freeze-dried amino acids, as well as their tendency to form complexes with other ingredients.[6] Many amino acids are considered to protect proteins basically in similar mechanisms with disaccharides. They thermodynamically stabilize protein conformation in aqueous solutions and probably in frozen solutions by being preferentially excluded from the immediate surface of proteins.[7] Glass-state amorphous solids formed by freeze-drying of the disaccharides or some amino acids protect proteins from structural changes thermodynamically by substituting surrounding water molecules.[8] They also reduce chemical degradation of freeze-dried proteins kinetically by reducing the molecular mobility.[2,8] In addition, some amino acids (*e.g.*, L-arginine) also prevent protein aggregation in aqueous solutions prior to the drying process and after reconstitution.[9] Choosing appropriate counterions that form glass-state solid should be one of the key factors in designing amino acid-based amorphous freeze-dried formulations.[10,11] For example, glass transition temperatures (T_g) of freeze-dried L-histidine salts depend largely on the counterions.[12] Co-lyophilization of L-arginine and multivalent inorganic acids (*e.g.*, H_3PO_4, H_2SO_4) results in glass-state amorphous solids that protect proteins during the process and storage (*e.g.*, tissue plasminogen activator formulation, PDR 2003).[13] Some organic acid and inorganic cation combinations (*e.g.*, sodium citrates) also form high glass transition temperature amorphous solids.[14] Various functional groups (*e.g.*, amino, carboxyl, hydroxyl) in the constituting molecules contributes significantly to form the glass-state amorphous salt solids.[15] Producing glass-state amorphous solids by freeze-drying of amino acid and organic acid combinations, and their application in pharmaceutical formulations are interesting topics to explore.[15]

The purpose of this study was to produce stable amorphous solids that protect proteins by freeze-drying combinations of amino acids and organic acids. The physical properties of frozen solutions and freeze-dried solids containing the popular excipients and model chemicals were studied. The effect of the excipient combinations on the freeze-drying of lactate dehydrogenase (LDH) was also examined.

Experimental

Materials LDH (rabbit muscle) was obtained from Sigma Chemical (St. Louis, MO, U.S.A.). Succinic acid was produced by Kanto Chemical Co. (Tokyo, Japan). L-(+)-Tartaric acid, DL-malic acid, and other chemicals were of analytical grade and were purchased from Wako Pure Chemical (Osaka, Japan). The protein solutions were dialyzed against 50 mM sodium phosphate buffer (pH 7.0), and then centrifuged (1500 *g* × 5 min) and filtered (0.45 μm, polyvinyliden difluoride (PVDF), Millipore) to remove insoluble aggregates before the freeze-drying study.

Freeze-Drying A pH meter (HM-60G, TOA-DKK Co., Tokyo, Japan) was used to determine the pH of the aqueous solutions at 25 °C. A freeze-drier (Freezvac 1C, Tozai-Tsusho, Tokyo, Japan) was used to lyophilize the aqueous solutions. Aliquots of aqueous solutions (250 μl) in flat-bottom glass vials (10 mm diameter) were frozen by immersion in liquid nitrogen. The solutions were freeze-dried without shelf temperature control (20 h), and then at 35 °C (8 h). Solid samples for diffuse-reflection near-infrared analysis were prepared by freeze-drying the aqueous solutions (2 ml) in glass vials (21 mm diameter).

Thermal Analysis Thermal analysis of frozen solutions and dried solids

* To whom correspondence should be addressed. e-mail: Izutsu@nihs.go.jp

was performed using a differential scanning calorimeter (DSC) (Q-10, TA Instruments, New Castle, DE, U.S.A.) and software (Universal Analysis 2000, TA Instruments). Aliquots of aqueous solutions (10 μl) in aluminum cells were cooled from room temperature at 10 °C/min, and then scanned from −70 °C at 5 °C/min. The effect of heat-treatment (annealing) on the thermal properties of the frozen solutions was studied after the initial heating scan paused at −10 °C, then the samples were maintained at this temperature for 10 min. Thermal data were acquired in the subsequent heating from −70 °C at 5 °C/min. Freeze-dried solids (1—2 mg) in hermetic aluminum cells were subjected to the thermal analysis from −20 °C at 5 °C/min under nitrogen gas flow. Melted organic acids (approx. 5 mg, 200 °C) in aluminum cells were rapidly cooled to −50 °C, and then scanned at 5 °C/min to obtain the glass transition temperatures. Glass transition temperatures were determined as the midpoint (maximum inflection) of the discontinuities in the heat flow curves.

Powder-X-Ray Diffraction (XRD) The powder X-ray diffraction patterns were measured at various temperatures by using a Rint-Altima diffractometer (Rigaku, Tokyo, Japan) with Cu$K\alpha$ radiation at 40 kV/40 mA. The samples were scanned in the area of $5° < 2\theta < 35°$ at an angle speed of 15°/min by heating at 2 °C/min from room temperature.

Mid- and Near-Infrared Analysis A Fourier-transform infrared spectrophotometer (MB-104, Bomen, Quebec, Canada) with a gas generator (Balston, Haverhill, MA, U.S.A.) and Grams/32 software were used to obtain mid-infrared spectra of freeze-fried solids. Approximately 0.5 mg of the solid was mixed with dried KBr powder (250 mg) and made into tablets by compression. The KBr tablets were scanned 128 times to obtain the spectra in the 400—4000 cm^{-1} region. Near-infrared spectroscopy was performed by using a Bruker MPA system with a diffuse-reflectance integrating-sphere probe (PbS detector) and OPUS software (Ettlingen, Germany). Near-infrared light was directed upward from the bottom of the glass vials containing freeze-dried solids to obtain the reflected signal over a range of 4000—12000 cm^{-1} with a resolution of 4 cm^{-1} in 128 scans. The freeze-dried solids were measured twice by rotating the sample vials between measurements.

Activity of Lactate Dehydrogenase in Freeze-Dried Solids Aqueous solutions (250 μl) containing LDH (0.05 mg/ml) and excipients were freeze-dried in flat-bottom glass vials (10 mm diameter). One of the enzyme solutions was freeze-dried at a higher sodium phosphate buffer concentration (50 mM, pH 7.0). Other enzyme solutions contained the added excipients and lower concentration buffer components (<1 mM) diluted from the dialyzed protein solutions. Activity of LDH was obtained spectrophotometrically at 25 °C. Each 1.0 ml of assay mixture contained 0.35 mM pyruvic acid and 0.07 mM reduced nicotinamide-adenine dinucleotide (NADH) in 50 mM sodium phosphate buffer (pH 7.5). The enzyme reaction was started by the addition of LDH solution (50 μl), and the decrease in the absorbance at 340 nm was monitored. The enzyme activity (%) relative to that before freezing was shown.

Results

Physical Property of Frozen Solutions The thermal profiles of frozen solutions containing L-histidine and citric acid at various concentration ratios (total 200 mM) are shown in Fig. 1. The single-solute frozen L-histidine solution (200 mM) showed a T_g' (glass transition temperature of maximally freeze-concentrated solute) at −33.5 °C, and an exotherm peak that suggests eutectic crystallization at around −8 °C.[12] Freeze-drying of solutions at above their T_g' often induces physical collapse because of the significantly reduced local viscosity in the freeze-concentrated phase.[1] The second scan of the 200 mM L-histidine solutions after the heat-treatment (−10 °C, 10 min) gave flat thermograms that indicate crystallized solute up to the ice melting temperature (data not shown). The citric acid solution (200 mM) had a T_g' at −55.1 °C, indicating that the solute remained amorphous in the freeze-concentrated phase surrounding ice crystals. The L-histidine crystallization peak disappeared in the presence of citric acid. The two-solute frozen solutions showed transitions (T_g's) at temperatures as high as −22.8 °C at the equal (100 mM) L-histidine and citric acid concentrations.

Figure 2 shows transition temperatures (T_g') of frozen solutions containing amino acids and organic acids at various concentration ratios. Some single-solute frozen amino acid or organic acid solutions (200 mM) had apparent T_g' transitions at −44.2 °C (L-arginine), −55.1 °C (citric acid), and

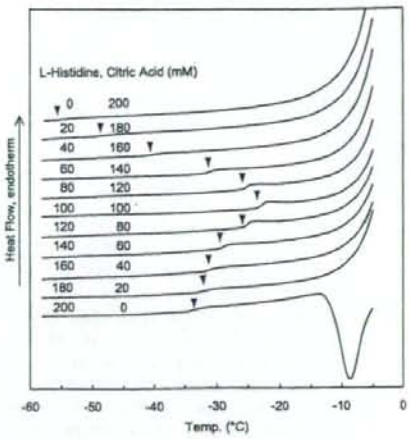

Fig. 1. Thermal Profiles of Frozen Solutions Containing L-Histidine and Citric Acid

Aliquots (10 μl) of solutions in hermetic aluminum cells were scanned from −70 °C at 5 °C/min. Glass transition temperatures of maximally freeze-concentrated solutes (T_g') are indicated by inverted triangles (▼).

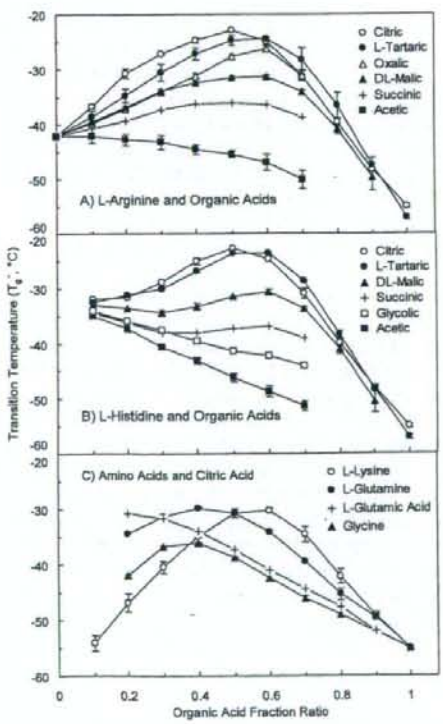

Fig. 2. Glass Transition Temperatures of Maximally Freeze-Concentrated Solute (T_g') in Frozen Solutions Containing an Amino Acid and an Organic Acid at Varied Concentration Ratios (Total 200 mM, Average±S.D., $n=3$)

−57.1 °C (L-tartaric acid). The frozen L-glutamine solution showed both T'_g (−42.8 °C) and the subsequent eutectic crystallization peak (approx. −25 °C) in the heating scan (data not shown). Thermograms of the frozen L-lysine and DL-malic acid solutions inclined gradually without apparent transition up to the ice melting endotherm, which suggested T'_gs lower than −60 °C. Exotherm peaks either in the cooling process (glycine, acetic acid) or in the heating scan (oxalic acid) indicated eutectic crystallization in the frozen solution.[16] Potential T'_g transitions of some frozen solutions that also showed eutectic crystallization peaks (*e.g.*, 200 mM L-histidine or L-glutamine) were not included in the figure. The limited solubility of some amino acids and organic acids (*e.g.*, L-glutamic acid, fumaric acid, maleic acid) prevented them from undergoing thermal analysis at 200 mM. A lower concentration glutamic acid solution (100 mM) showed a T'_g at −32.2 °C and an exotherm peak that suggests eutectic crystallization at around −11.0 °C (data not shown).

Mixing of the solutes induced some unique physical properties in the frozen solutions that depend on the number of functional groups in the consisting molecules. The transition temperatures (T'_gs) of frozen solutions containing a basic or neutral amino acid (L-histidine, L-arginine, L-lysine, L-glutamine, glycine) and a hydroxy di- or tricarboxylic acid (citric acid, L-tartaric acid, DL-malic acid) showed bell-shaped profiles. The frozen solutions containing a hydroxy di- or tricarboxylic acid (citric acid, L-tartaric acid) and an acidic amino acid (L-glutamic acid) did not show the mixing-induced upward T'_g shift. Citric acid also effectively prevented the crystallization of glycine in the frozen solutions. Dicarboxylic acids (succinic acid, maleic acid, fumaric acid, oxalic acid) showed a high tendency to crystallize in the single-solute frozen solutions and in some mixture frozen solutions.[15,17] The frozen solutions containing L-arginine and oxalic acid or succinic acid also presented the high transition temperature (T'_g) by mixing. A mono-carboxylic acid (acetic acid), a hydroxy mono-carboxylic acid (glycolic acid), and HCl did not show the upward T'_g shift in the mixture with the basic amino acids.[13]

Physical Property of Freeze-Dried Solids Freeze-drying of the single-solute amino acid solutions resulted in cylindrical cakes that showed varied crystallinity in the powder X-ray diffraction (XRD) and thermal analyses (Figs. 3, 4). Freeze-dried L-arginine showed the typical harrow XRD pattern of amorphous solids. Thermal scan of the solid showed the glass transition (52.6 °C) and subsequent crystallization exotherm (105—110 °C). Freeze-dried L-histidine showed largely amorphous XRD pattern (30 °C) with the broad glass transition (65—100 °C) and crystallization at varied temperatures (120—150 °C). The L-arginine and L-histidine solids showed apparent crystallization peaks in the XRD patterns at the elevated temperature (150 °C). The dried L-glutamine (200 mM) solids showed features of both crystalline (*e.g.*, peaks in the XRD pattern) and amorphous (*e.g.*, glass transitions and heat-induced crystallization exotherm) solids. The solute concentration in the initial solution and thermal history in the freeze-drying process should determine the crystallinity of the freeze-dried L-histidine and L-glutamine.[12] Glycine was freeze-dried as β polymorph crystal.[18] Freeze-drying of citric acid or L-tartaric acid solutions (200 mM) resulted in unstructured or particulate solids that

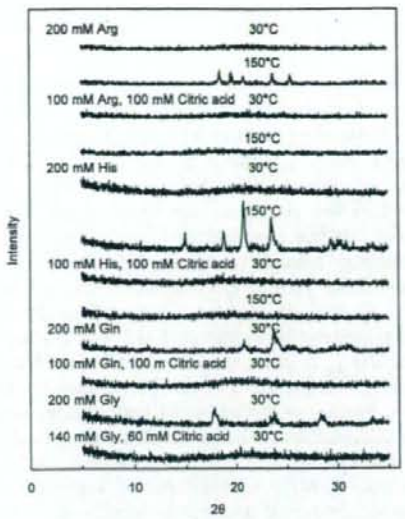

Fig. 3. Powder X-Ray Diffraction Patterns of Freeze-Dried Solids Containing Amino Acids and Citric Acid

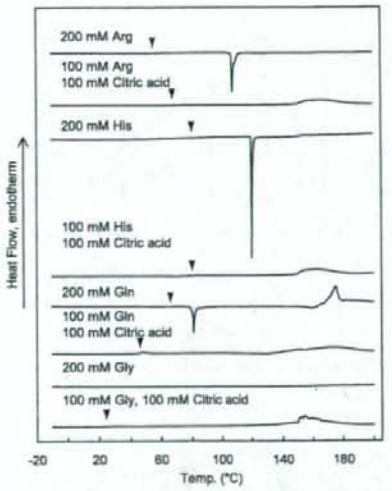

Fig. 4. DSC Thermograms of Freeze-Dried Solids Containing Amino Acids and Citric Acid

Freeze-dried solids (1—2 mg) in hermetic aluminum cells were scanned from −20 °C at 5 °C/min.

indicate physical collapse in the primary during process. Amorphous solids of the organic acids prepared by rapid-cooling of the melt liquid showed glass transition at 9.2 °C (citric acid) and 68.1 °C (L-tartaric acid) in the thermal scan (n=3).[19]

Co-lyophilizing the basic or neutral amino acids (L-arginine, L-histidine, L-glutamine, glycine) and the organic acid (citric acid, L-tartaric acid) produced cylindrical non-crystalline cake solids at wide initial concentration ratios (Figs. 3—5). The solids obtained by freeze-drying the basic amino acids (L-arginine, L-histidine) with citric or L-tartaric acid showed glass transition at temperatures (T_gs) much higher

than those of the individual components. The transitions were observed at temperatures as high as 89.5 °C (140 mM L-arginine, 60 mM citric acid) or 98.5 °C (160 mM L-histidine, 40 mM citric acid). Shrinking of some solids containing higher ratio of organic acid during the freeze-drying process suggested their low glass transition temperatures. The XRD and thermal analysis also indicated that the co-lyophilized solids remained amorphous up to 150 °C. Some binary freeze-dried solids showed a broad endotherm that suggests component decomposition at the elevated temperatures. The mixing of L-arginine with citric acid and with L-tartaric acid showed similar T_g profiles, in spite of the large difference in their transition temperatures of the cooled-melt solids. The bell-shaped profiles of the transition temperatures were significantly different from the reported transitions of binary nonionic molecule systems that follow Gordon–Taylor equation.[20] Glass transition temperatures of amorphous solids containing ideally mixed nonionic molecules without particular attractive or repulsive interactions shift between those of the individual components. Contrarily, the glass transition temperatures of co-lyophilized L-glutamine and citric acid combination solids shifted linearly between those of the individual components, which suggested absence of the particular attractive interactions between the heterogeneous molecules in the solids. Co-lyophilization of glycine and citric acid resulted in amorphous cake solids only at limited molar ratios.

Transition temperatures (T_g', T_g) of the excipient combinations obtained at a fixed (0.1) molar ratio interval were plotted against the pH of the initial solutions (25 °C, Fig. 6). Some mixtures (*e.g.*, L-arginine and citric acid, L-histidine and citric acid) yielded high T_g' frozen solutions and high T_g freeze-dried solids from weakly acidic initial solutions ($-35\,°C < T_g'$, $80\,°C < T_g$, pH 4—6), which are preferable in parenteral protein formulations. Small changes in the L-arginine and organic acid compositions (0.1 molar fraction) significantly shifted pH at the neutral region.

The mid- and near-infrared spectra of the freeze-dried L-arginine and citric acid combinations showed broad absorption bands that are typical of amorphous solids (Figs. 7, 8).[21] Co-lyophilization with citric acid reduced an amino group absorption band of L-arginine at 1550 cm^{-1} in the mid-IR spectra (KBr method), indicating altered environment of the functional group. Similar reduction of the amino group band has been reported in L-arginine–HCl salt crystal and L-argi-

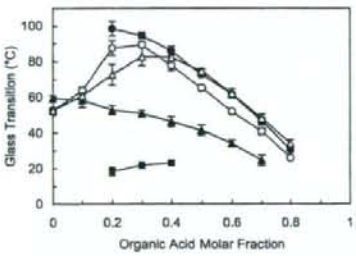

Fig. 5. Glass Transition Temperatures of Freeze-Dried Binary Solids

Each symbol denotes transition of solids containing L-arginine and citric acid (○), L-arginine and tartaric acid (△), L-histidine and citric acid (●), L-glutamine and citric acid (▲), or glycine and citric acid (■) (total: 200 mM, average ± S.D., $n=3$).

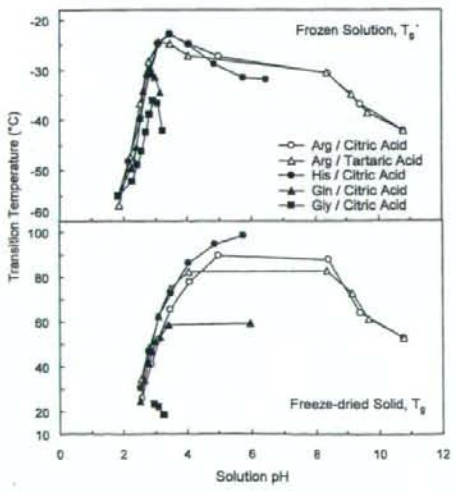

Fig. 6. Effect of Initial Solution pH (25 °C) on the Transition Temperatures of Frozen Solutions (T_g') and Freeze-Dried Solids (T_g) Containing an Amino Acid and an Organic Acid at a Fixed (0.1) Molar Concentration Ratio Intervals (200 mM Total, $n=3$)

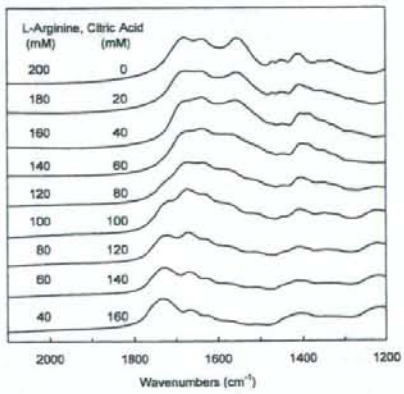

Fig. 7. Mid-Infrared Spectra of Freeze-Dried L-Arginine and Citric Acid Combinations Obtained by a KBr Tablet Method (128 Scans)

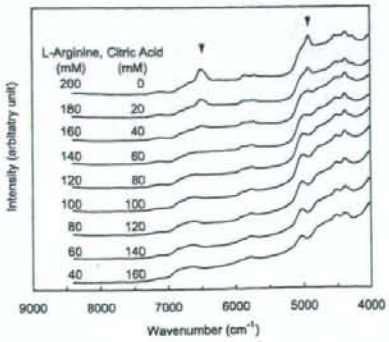

Fig. 8. Diffuse-Reflection Near-Infrared Spectra of Freeze-Dried L-Arginine and Citric Acid Combinations Obtained at the Bottom of the Glass Vials (128 Scans)

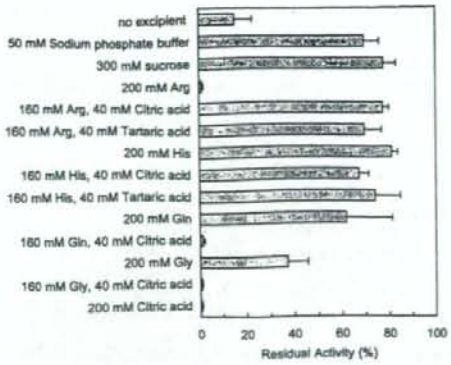

Fig. 9. Effect of Amino Acid and Organic Acid Combinations on the Activity of Freeze-Dried Lactate Dehydrogenase (50 μg/ml, Average±S.D., $n=3$)

nine freeze-dried with inorganic acids (*e.g.*, HCl, H_3PO_4).[13] A carboxyl group band at 1725 cm^{-1} appeared when the citric acid ratio was increased. Diffuse-reflection near-infrared spectra obtained non-destructively at the bottom of the glass vials also indicated the altered local environment of the functional groups. A large amino band of L-arginine (6505 cm^{-1}, N–H stretching 1st overtone) disappeared in the presence of lower molar concentration ratio of citric acid in the initial solution (140 mM L-arginine, 60 mM citric acid). Increasing the citric acid ratio also reduced the large absorption band at 4920 cm^{-1}, and concomitantly induced band at 5030 cm^{-1} in the co-lyophilized solids. Assignment of these bands remains to be elucidated. The results strongly suggested hydrogen-bonding and/or electrostatic interactions between L-arginine and citric acid in the lyophilized solids.

Effect of Excipients on Inactivation of Freeze-Dried LDH Freeze-drying of LDH in the absence of the stabilizing excipients resulted in significant reduction of the activity (approximately 15% of the initial solution) (Fig. 9). Higher enzyme activity was retained in freeze-drying at a higher phosphate buffer concentration (50 mM). Some amino acid and organic acid combinations that provide neutral to weakly acidic initial solution (pH 5—8) and amorphous dried solids also retained the enzyme activity. The enzyme lost most of the activity in freeze-drying from extreme pH solutions (*e.g.*, 200 mM L-arginine, pH 10.6). Addition of citric acid or L-tartaric acid slightly reduced the effect of L-histidine to retain the activity of LDH during freeze-drying. Crystallization of glycine in the single-solute frozen solution, and concomitant loss of the protecting effect, should explain the lower remaining enzyme activity.[1,2,22]

Discussion

The freeze-drying of aqueous solutions containing some basic or neutral amino acid (*e.g.*, L-arginine, L-histidine) and hydroxy di- or tricarboxylic acid (*e.g.*, citric acid, L-tartaric acid) combinations resulted in the glass-state amorphous solid cakes that protect proteins from dehydration stresses. Some of the solids showed glass transition temperatures comparable to those of disaccharides (*e.g.*, sucrose, trehalose).[4] The data and recent literature on the properties of related substances in different physical states (*e.g.*, complex crystals, ionic liquids) strongly suggested contribution of the multiple functional groups of the consisting molecules to form the interaction (*e.g.*, electrostatic, hydrogen-bonding) networks required for the glass-state amorphous solids.[23—25] Multiple amino, carboxyl, and hydroxyl groups in the solute molecules raise transition temperatures of the mixture frozen solutions (T_g') and the freeze-dried solids (T_g).[15] The ammonium carbohydrate ion pairs form multiple hydrogen-bondings in some non-polar solvents.[23,24] Differently protonated carboxyl and carboxylate groups also form an intermolecular hydrogen-bonding network.[25]

The amino acids and organic acids containing plural amino or carboxyl groups should have large chance to form the interactions with multiple counterpart molecules. The contribution of the multiple functional groups should explain the high transition temperatures (T_g', T_g) of the L-arginine and citric acid combination. L-Arginine also forms stable amorphous freeze-dried solids with multivalent inorganic acids (*e.g.*, H_3PO_4).[11,13] Frozen sodium citrate and tartrate buffer solutions exhibit the highest T_g' at certain sodium concentration ratios.[17] Supramolecular interactions (*e.g.*, peptide-like periodic interactions) reported in some complex crystals of amino acid and dicarboxylic acid (*e.g.*, L-arginine and adipic acid, X-ray analysis)[26] should support the possible multi-molecular interaction network in the less-ordered amorphous phase.

Hydroxyl groups in the citric acid, L-tartaric acid, and DL-malic acid should introduce additional hydrogen bonding to the amorphous phase. The number of hydroxyl groups in the component, and the accompanying change in the molecular interactions are major factors in determining the glass transition temperature of some ionic liquids composed of an amino acid and a 1-allylimidazolium cation.[27] The intense interactions and resulting reduction of the molecular mobility may prevent the crystallization of amino acids (*e.g.*, glycine, glutamine) at concentration ratios much lower than those of "inert" nonionic solutes (*e.g.*, sucrose) or inorganic salts (*e.g.*, NaCl).[17,30—32]

The high glass transition temperature amorphous solids formed by combinations of popular excipients would be a practical alternative to disaccharides in the design of freeze-dried protein formulations. The excipient combinations would satisfy the two major protein-stabilizing mechanisms postulated on saccharides, namely substitution of the surrounding water molecules by hydrogen-bonding and reduction of the chemical reaction by embedding in the glass-state solids.[6—8] Additional effects of some amino acids (*e.g.*, reduced aggregation in aqueous solution by L-arginine) preferable in protein formulations are also anticipated.[9] The limited crystallinity and low volatility of the amino acid and organic acid should reduce the risk of pH change and the resulting protein inactivation in the freeze-drying process reported in some buffer systems.[28]

Various proteins degrade during the freeze-drying process and subsequent storage through several chemical and physical mechanisms.[3,29] The low concentration LDH solution is often used as a model system for studying the effect of co-solutes in the freeze-thawing and freeze-drying processes because of its apparent tendency to lose its activity due to irreversible subunit dissociation and conformation change.[30] The ability of excipient combinations to retain the enzyme

activity in the freeze-drying process should indicate the stabilization of the quarterly structure against freeze-concentration and dehydration stress. Different molecular mobility, local pH, water content, and crystallinity of the excipients may affect the chemical degradation rate of the freeze-dried enzyme in the subsequent storage. The freeze-dried basic amino acid and organic acid combination solids should provide the embedded proteins with unique local environments that are significantly different from those of the nonionic excipients (*e.g.*, saccharides). The structural and chemical stability of proteins in these solids during the freeze-drying process and storage is an intriguing topic that needs further study through various model protein and stress systems.

References

1) Nail S. L., Jiang S., Chongprasert S., Knopp S. A., *Pharm. Biotechnol.*, **14**, 281—360 (2002).
2) Tang X., Pikal M. J., *Pharm. Res.*, **21**, 191—200 (2004).
3) Carpenter J. F., Arakawa T., Crowe J. H., *Dev. Biol. Stand.*, **74**, 225—238 (1992).
4) Franks F., *Dev. Biol. Stand.*, **74**, 9—18 (1992).
5) Lee J. C., Timasheff S. N., *J. Biol. Chem.*, **256**, 7139—7201 (1981).
6) Chang B. S., Randall C., *Cryobiology*, **29**, 632—656 (1992).
7) Arakawa T., Timasheff S. N., *Arch. Biochem. Biophys.*, **224**, 169—177 (1983).
8) Sane S. U., Wong R., Hsu C. C., *J. Pharm. Sci.*, **93**, 1005—1018 (2004).
9) Tsumoto K., Umetsu M., Kumagai I., Ejima D., Philo J. S., Arakawa T., *Biotechnol. Prog.*, **20**, 1301—1308 (2004).
10) Osterberg T., Fatouros A., Mikaelsson M., *Pharm. Res.*, **14**, 892—898 (1997).
11) Mattern M., Winter G., Kohnert U., Lee G., *Pharm. Dev. Technol.*, **4**, 199—208 (1999).
12) Osterberg T., Wadsten T., *Eur. J. Pharm. Sci.*, **8**, 301—308 (1999).
13) Izutsu K., Fujimaki Y., Kuwabara A., Aoyagi N., *Int. J. Pharm.*, **301**, 161—169 (2005).
14) Li J., Chatterjee K., Medek A., Shalaev E., Zografi G., *J. Pharm. Sci.*, **93**, 697—712 (2004).
15) Kadoya S., Izutsu K., Yonemochi E., Terada K., Yomota C., Kawanishi T., *Chem. Pharm. Bull.*, **56**, 821—826 (2008).
16) Akers M. J., Milton N., Byrn S. R., Nail S. L., *Pharm. Res.*, **12**, 1457—1461 (1995).
17) Shalaev E. Y., Johnson-Elton T. D., Chang L., Pikal M. J., *Pharm. Res.*, **19**, 195—201 (2002).
18) Chongprasert S., Knopp S. A., Nail S. L., *J. Pharm. Sci.*, **90**, 1720—1728 (2001).
19) Lu Q., Zografi G., *J. Pharm. Sci.*, **86**, 1374—1378 (1997).
20) Shamblin S. L., Taylor L. S., Zografi G., *J. Pharm. Sci.*, **87**, 694—701 (1998).
21) Yonemochi E., Inoue Y., Buckton G., Moffat A., Oguchi T., Yamamoto K., *Pharm. Res.*, **16**, 835—840 (1999).
22) Anchordoquy T. J., Carpenter J. F., *Arch. Biochem. Biophys.*, **332**, 231—238 (1996).
23) Sada K., Tani T., Shinkai S., *Synlett*, **2006**, 2364—2374 (2006).
24) Yerger E. A., Barrow G. M., *J. Am. Chem. Soc.*, **77**, 6206—6207 (1955).
25) Kobayashi N., Naito T., Inabe T., *Bull. Chem. Soc. Jpn.*, **76**, 1351—1362 (2003).
26) Roy S., Singh D. D., Vijayan M., *Acta Crystallogr. B*, **61**, 89—95 (2005).
27) Fukumoto K., Yoshizawa M., Ohno H., *J. Am. Chem. Soc.*, **127**, 2398—2399 (2005).
28) Li J., Guo Y., Zografi G., *Pharm. Res.*, **19**, 20—26 (2002).
29) Manning M. C., Patel K., Borchardt R. T., *Pharm. Res.*, **6**, 903—918 (1989).
30) Seguro K., Tamiya T., Tsuchiya T., Matsumoto J. J., *Cryobiology*, **27**, 70—79 (1990).